Growth of praseodymium oxide on Si(111) under oxygen-deficient conditions

A. Schaefer,[1,2] V. Zielasek,[1] Th. Schmidt,[2] A. Sandell,[3] M. Schowalter,[2] O. Seifarth,[4] L. E. Walle,[5] Ch. Schulz,[2] J. Wollschläger,[6] T. Schroeder,[4] A. Rosenauer,[2] J. Falta,[2] and M. Bäumer[1,*]

[1]*Institute of Applied and Physical Chemistry, University of Bremen, Leobener Str. NW2, D-28359 Bremen, Germany*

[2]*Institute of Solid State Physics, University of Bremen, P.O. Box 330440, D-28334 Bremen, Germany*

[3]*Department of Physics and Materials Science, Uppsala University, P.O. Box 530, SE-75121 Uppsala, Sweden*

[4]*IHP, Im Technologiepark 25, D-15236 Frankfurt (Oder), Germany*

[5]*Department of Physics, Norwegian University of Science and Technology, NO-7491 Trondheim, Norway*

[6]*Department of Physics, University of Osnabrück, Barbarastrasse 7, D-49069 Osnabrück, Germany*

(Received 5 February 2009; revised manuscript received 19 May 2009; published 15 July 2009)

Surface science studies of thin praseodymium oxide films grown on silicon substrates are of high interest in view of applications in such different fields as microelectronics and heterogeneous catalysis. In particular, a detailed characterization of the growth and the final structure of the films are mandatory to achieve a fundamental understanding of such topics as oxygen mobility and defect structure, and their role for the electronic and chemical properties. In this paper, the MBE growth of praseodymium oxide films on Si(111) substrates was investigated at low-deposition rates (0.06 nm/min) and low-oxygen partial pressures ($p(O_2) < 1 \times 10^{-10}$ mbar). To obtain insight into the structure and chemical composition of the growing film, spot profile analyzing low-energy electron diffraction (SPA-LEED), transmission electron microscopy, and synchrotron radiation-based x-ray photoelectron spectroscopy (XPS) and x-ray absorption spectroscopy (XAS) were applied. SPA-LEED reveals the formation of an initial closed layer followed by continuous roughening and formation of ordered three-dimensional structures. This result is in contrast to observations at higher-deposition rates, were a layer-by-layer growth was reported. XAS and XPS provide evidence that a continuous reaction takes place in the growing Pr_2O_3 film leading to the formation of silicate and silicide structures within the film. Combining all data, a consistent picture of the deposition of praseodymium oxide on Si(111) emerges which clearly shows that in contrast to higher-throughput molecular beam epitaxy conditions the reactivity of the growing film strongly influences the growth behavior at low-deposition rates and low pressures.

DOI: 10.1103/PhysRevB.80.045414 PACS number(s): 68.35.Ct, 81.15.−z, 61.05.J−, 82.80.Pv

I. INTRODUCTION

Oxide materials play an important role in many fields of technology. Rare earth oxides (REOs), for example, have received attention in such different fields as microelectronics and catalysis. Yet, the performance of REOs in these two areas and the range and the limitations of their application are determined by the same physical and chemical properties of these oxides. It is in particular the ability of the REOs to release oxygen from the lattice and the creation of oxygen vacancies,[1–3] which need to be understood and controlled.

Among the REOs, praseodymium oxides take up a special position as they exhibit the highest-oxygen mobility in the series.[4] In microelectronics, these materials are, e.g., of interest as versatile heteroepitaxy buffer layers to achieve the global integration of alternative semiconductors (e.g., Ge) on the Si material platform in the field of so-called engineered Si wafers. Here, the defects in the oxygen sublattice have a strong impact on the electric and electronic properties of the heteroepitaxial oxide buffer structure.[5,6]

Regarding their chemical behavior, praseodymium oxides are known to be catalytically active in a variety of reactions such as CO and NO oxidation,[7–9] dehydration, dehydrogenation,[10] or alkylation of organic compounds.[11] Since lattice oxygen is involved in these redox reactions taking place at the surface according to the Mars-van-Krevelen mechanism, the high-oxygen mobility and storage capability are important. In contrast to a Langmuir-Hinshelwood mechanism, the oxidation and reduction are spatially decoupled: the reoxidation of the oxide is not directly linked to the oxidation of adsorbates and can take place at different surface sites. The activity of such catalysts is thus directly connected to the mobility of oxygen vacancies in the lattice.

Due to this coupling of surface and bulk processes, it is obvious that the lateral dimensions of the oxides have an influence on the properties. Recently, it was shown, for instance, that the activity for catalytic CO oxidation depends on the synthesis method and the structure of the praseodymium oxides on the nanoscale.[12] Nanocrystalline samples exhibited a significantly higher activity than coarse grained material. In microelectronics, very often layers of just a few nanometers are grown. Therefore, redox-active adsorbates which cannot be avoided in the preparation under ambient conditions are expected to exert a non-negligible influence on the density of oxygen vacancies and thus on the electric and electronic properties making thus the controlled preparation of nanoscaled dielectrics difficult.

To obtain insight into the atomic details of the interaction of nanometer-sized REO materials with adsorbed molecules, studies of thin oxide films prepared on conductive substrates are ideal to elucidate the surface chemistry and physics as a function of the oxidation state of the oxide, as shown in a number of cases.[13–15] In particular, heteroepitaxial praseodymium sesquioxide (Pr_2O_3) films on silicon substrates are promising as models for Pr-Oxide-based nanoscale systems. Not only do they allow studying the properties of different phases of Pr_2O_3, namely, hexagonal (hex-Pr_2O_3) and cubic

Pr_2O_3 (cub-Pr_2O_3), but Pr_2O_3 in the cubic phase can further be oxidized to single crystalline PrO_2 (Ref. 16) so that different stoichiometries are accessible as well.

Most of the work on Pr oxide films grown on silicon substrates published so far was motivated by applications in microelectronics. In particular, the epitaxial growth of cubic (space group Ia-3) and hexagonal (space group P3m1) praseodymium sesquioxide were studied intensively on Si(001) and Si(111), respectively.[17–27] The first praseodymium sesquioxide films on Si(111) were prepared by Tarsa *et al.*,[25] using pulsed laser deposition (PLD). Later, the successful growth by molecular beam epitaxy (MBE) was shown.[24] On Si(001), the growth of cubic Pr_2O_3 films with (101) orientation was observed (for more details see Refs. 21–23, 26, and 27). The cub-Pr_2O_3 phase is thermodynamically more stable than the hex-Pr_2O_3 phase. However, on Si(111) the growth of the (0001)-oriented, high-temperature hex-Pr_2O_3 phase is favored due to the better match of the lattice of hex-Pr_2O_3 with the substrate lattice. The lattice mismatch is only 0.5% compared to ~3% for (111)-oriented cub-Pr_2O_3. Only when annealing hex-Pr_2O_3 films on Si(111) to 600 °C at elevated oxygen ($p(O_2)=1\times10^{-5}$ mbar) or nitrogen ($p(N_2)=1$ bar) pressures, a phase transformation to the cubic, (111) oriented Pr_2O_3 structure is observed.[24,28]

Whereas most of the studies reported in the literature dealt with films grown under high-vacuum conditions (pressures of 10^{-8} mbar and above), only in a few studies ultrahigh-vacuum conditions and correspondingly low-oxygen partial pressures were applied during the preparation. In view of results of Schmeißer *et al.* who, on the basis of theoretical calculations, predicted that silicide formation should be observed under oxygen-deficient conditions,[29] such conditions may alter the growth and the quality of the film.

Recently, we investigated the growth of hex-Pr_2O_3(0001) films on Si(111) using MBE and pressures of 10^{-8} mbar in connection with a relatively high-deposition rate of 6 nm/min.[17] As the main result we found that the hex-Pr_2O_3(0001) phase grows epitaxially in a layer-by-layer fashion up to a thickness of 12 nm. Just a thin praseodymium silicate layer is formed at the substrate interface. Libralesso *et al.*[19] and Jeutter *et al.*[18] reported the direct growth of a hex-Pr_2O_3 monolayer on the Si(111) substrate at lower-deposition rates and lower-ambient pressures. In the former study, the initial stages of Pr_2O_3 growth on Si(111) up to the first monolayer were investigated by scanning tunnel microscopy (STM) and low-energy electron diffraction (LEED).[19] That study revealed the formation of triangular islands in the submonolayer range.

In order to shed light on the question of how the preparation conditions influence the growth and whether preparations under UHV conditions are suitable to obtain smooth Pr_2O_3 films, we have applied a variety of methods in the present study. For structural analysis during growth, spot profile analyzing low-energy electron diffraction (SPA-LEED) was performed. In addition, synchrotron radiation (SR)-based x-ray photoelectron (XPS) and x-ray absorption spectroscopy (XAS) were used to monitor the chemical composition of the growing oxide layer in detail. To complete the picture, cross-sectional scanning transmission electron microscopy (STEM) was employed to obtain structural information about the film and in particular the interface region. On the basis of all results, we are able to provide a consistent picture of praseodymium oxide growth on Si(111) at low-oxygen partial pressures and low-deposition rates.

II. EXPERIMENTAL DETAILS

As substrate, phosphorous-doped Si(111) ($\rho<0.005$ Ω cm) with a miscut angle $<0.2°$ was used. After insertion into the UHV chamber, the samples were heated at 600 °C for a minimum of 12 h. Then they were annealed rapidly by direct current heating up to 1250 °C for several times in order to obtain a clean (7×7) reconstructed Si(111) surface. The temperature was measured using an infrared pyrometer. The praseodymium oxide was deposited by electron beam evaporation. The ambient pressure during deposition was below $5\cdot10^{-10}$ mbar at all times which is a very low-background pressure (corresponding also to a low-oxygen partial pressure) compared to other studies where the films were prepared with higher-deposition rates. A noncommercial evaporator setup was used filled with Pr_6O_{11}. Note that Pr_6O_{11} is reduced to Pr_2O_3 after annealing in UHV. In the gas phase the main species found is PrO forming stoichiometric Pr_2O_3 on Si(111) surface in the temperature range of 500 °C to 625 °C.[2,20]

The same evaporator setup was used in all experiments reported in the following. The rate of material deposition was determined by deposition on a quartz microbalance. An estimate for the oxide coverage has also been obtained by evaluating the attenuation of the Si 2p core level signal in XPS. The deposition rate revealed by these methods was in the range of 0.06 nm/min, assuming that a smooth hex-Pr_2O_3 layer forms. This is in excellent agreement with the film thicknesses estimated by TEM.

The high-resolution diffraction experiments where conducted in a single UHV chamber using an Omicron SPA-LEED system (For information about the spot profile analyzing method see Refs. 30–32). The base pressure was below 10^{-10} mbar. In order to monitor the specular LEED beam [i.e., the (00)-spot] intensity during oxide deposition, the molecular beam had an incident angle of about 30° with respect to the sample surface while the electron beam had near normal incidence.

The XPS/XAS measurements were performed at beamline D1011 of the MAX-lab synchrotron radiation source in Lund, Sweden. The Si(111) substrates were flash-annealed in a preparation chamber until no oxygen and no carbon signal were detected by XPS. After depositing praseodymium oxide, the samples were transferred to an analysis chamber housing a SCIENTA SES200 energy analyzer (pressure during analysis typically $<2\times10^{-10}$ mbar). In case of XPS, the spectra were recorded under normal emission. The binding energy scale was referenced to the Fermi level of a Pt foil via the Si 2p bulk signal. X-ray absorption spectroscopy was performed in the total electron yield mode. In this mode, the information depth is larger than in XPS and thus information on almost the whole film is obtained. The absolute photon energy was determined using photoemission spectra recorded with first and second order light.

For the TEM experiments a sample with a 14 nm thick praseodymium oxide layer on Si(111) was prepared in UHV and then shaped into a TEM specimen using a Tripod method and edged in a GATAN precision ion-polishing system using Ar ions under an incidence angle of 4°. TEM investigations were carried out using a FEI Titan 80/300 equipped with an imaging Cs corrector. The specimen was oriented in such a way that the electron beam was aligned parallel to the [1–10] direction of the Si substrate and Z-contrast images were taken with a high-angle annular dark-field (HAADF) detector in scanning mode.

III. RESULTS AND DISCUSSION

In this section, results on the structure and morphology of the growing film as determined by SPA-LEED will be discussed first, providing information on the growth mode as well as on lateral and vertical roughness. Then, details on the chemical composition of the growing film obtained by XPS and XAS will be presented which also give insight into the coordination of oxygen in the film. Results of a cross-sectional STEM study on the morphology of a 14 nm thick film will be shown last. All structural and chemical data together lead to a consistent picture of the evolution of the structure and composition of the surface layer that develops upon deposition of Pr oxide on Si(111) at low-oxygen partial pressures.

SPA-LEED

In a first experiment, the intensity of the specular (00) reflection in a low-energy electron diffraction experiment was monitored continuously during oxide deposition. The electron energy (E=97 eV) was chosen in such a way that destructive interference would occur for scattering from (0001)-oriented hex-Pr_2O_3 layers separated by step heights that correspond to the vertical lattice constant c =0.6016 nm of the hexagonal unit cell in (0001) direction. Therefore, intensity oscillations of the specular reflection should be observed during deposition of the first layers if the oxide grows in a layer-by-layer fashion as recently observed in a study using MBE (ref. 17). Maximum intensity would be observed upon completion of each new layer, in analogy to reflection high-energy electron diffraction (RHEED) experiments.[17,31,33] In contrast to the RHEED, the electron beam was kept at almost normal incidence while the oxide was deposited under an angle of ~30° with respect to the substrate surface plane.

Figure 1 displays the results of intensity measurements recorded during continuous deposition at 550 °C and 625 °C substrate temperature, respectively. The intensity of the specular beam for growth at 625 °C shows the clear parabolic behavior (minimum at 0.3 nm, maximum at 0.6 nm) expected for laminar growth in heteroepitaxy with a completed monolayer after deposition of 0.6 nm oxide,[34,35] which is close to the vertical lattice constant of hex-Pr_2O_3 in (0001) direction.[2] The thickness of two atomic layers of the (111)-oriented cub-Pr_2O_3 phase (0.644 nm) is somewhat larger but would also fit within the experimental margin of

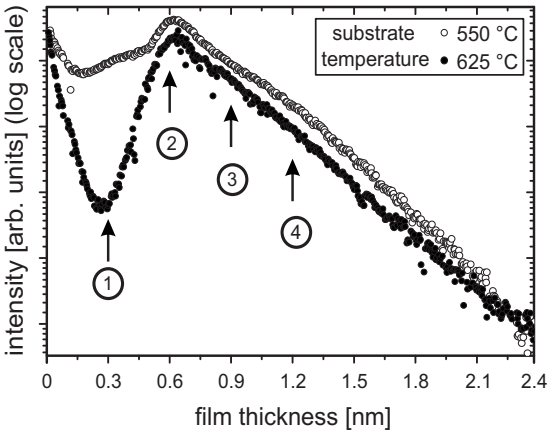

FIG. 1. Intensity of the specular beam (logarithmic scale) during oxide deposition recorded at 97 eV beam energy and 550 °C (open circles) and 625 °C (filled circles) substrate temperature, respectively. The numbers denote points at which 2D diffraction patterns and spot profiles (Figs. 2–4) were taken during stepwise deposition.

error, taking into account only the specular reflection data. For deposition at 550 °C, the coverage dependence of the specular intensity shows a minimum at 0.2 nm and a plateau at 0.4 nm indicating that the oxide film does not grow with the full height of the hex-Pr_2O_3 bulk unit cell [or two atomic (111) layers of cub-Pr_2O_3], initially. Nevertheless, the maximum at 0.6 nm proves that a flat Pr_2O_3 monolayer is only completed at that thickness. Upon further oxide deposition, the surface does *not* grow layer-by-layer but increasingly roughens as indicated by a continuous exponential decrease in the specular intensity. (Note that the overall lower-specular intensity at 625 °C can be attributed to increased thermal diffuse scattering.[36])

The labels 1 to 4 in Fig. 1 denote oxide coverages at which a more detailed analysis of the LEED spot profiles was performed in order to gain more insight into the morphology and long-range order of the growing oxide film. For this purpose, Pr oxide was deposited under normal incidence of the molecular beam in a stepwise fashion on a freshly prepared Si(111) surface. After each deposition step, the sample was cooled down to room temperature and two-dimensional high-resolution maps of the (00) diffraction spot as well as profile scans through the (00) spot were recorded. Figure 2 shows the (00) spot of a sample prepared at 550 °C substrate temperature. The grayscale (colored online) representation is chosen to emphasize the shape of the diffraction spot. Maps of the (00) spot after deposition of oxide with a nominal film thickness of 0.3 and 0.6 nm, respectively, are shown in Fig. 2(a) for different electron energies. As discussed before, completion of the initial smooth layer was observed at a film thickness of ~0.6 nm. At a coverage of half the initial layer (~0.3 nm nominal oxide thickness) the (00) spot exhibits a pronounced threefold symmetry. The shape is most pronounced at an electron energy of ~95.5 eV which corresponds to a condition of maximum constructive interference of scattering at adjacent silicon substrate terraces, rendering substrate steps invisible to LEED. Therefore, the three-fold symmetry of the diffraction spot must be caused by the incomplete first oxide layer. A faceting of the

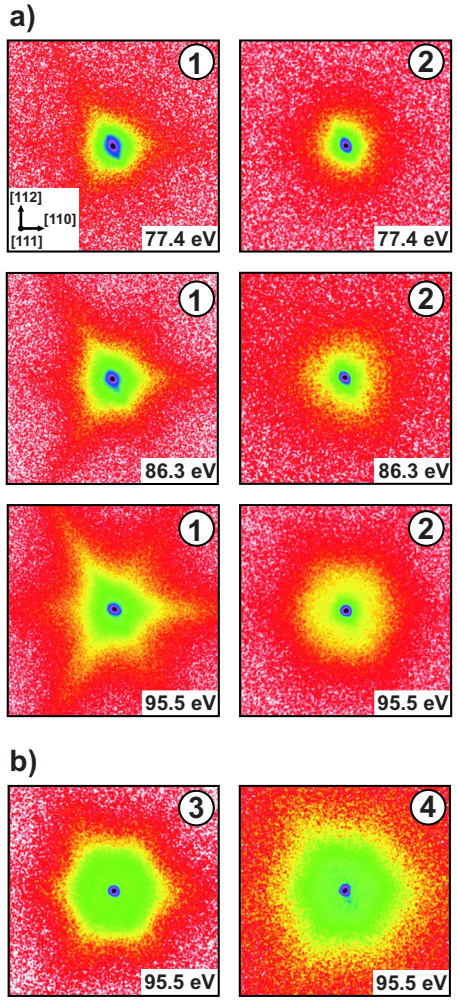

FIG. 2. (Color online) 2d diffraction maps of the specular beam (logarithmic scale for intensity) after oxide deposition at 550 °C substrate temperature. The numbers correspond to the deposition step at which the data were taken according to Fig. 1. Each frame shows a reciprocal area of 20%Bz×20%Bz (1% Brillouin zone $=2\pi/384$ Å^{-1}). Maps recorded (a) after the first two deposition steps at different electron energies as indicated in each frame and (b) at higher coverages at 95.5 eV electron energy.

surface can be excluded as reason for the (00) spot shape because in that case the triangular extensions of the spot should evolve into satellites with varying distance from the (00) reflection as the electron energy is varied.[31] This is not observed in our experiments. In fact, islands with triangular shape have been observed by Libralesso *et al.* under similar growth conditions by STM.[19] Since pure 2D diffraction from triangular islands leads to diffraction patterns of six-fold symmetry, we attribute the threefold symmetry of the diffuse intensity to the breaking of the three-fold diffraction symmetry of the Si(111) substrate due to the Pr_2O_3 islands.[37]

At the intensity maximum in Fig. 1 (label 2), i.e., after completion of the initial smooth layer, the corresponding diffraction pattern of the (00) spot is very sharp and exhibits an almost round shape. On a larger scale (not shown), first order spots are observed at positions consistent with the Si(111) substrate. Obviously, the initial layer is not only smooth and complete but also pseudomorphic with respect to the substrate. The pattern exhibits hexagonal symmetry as expected for the hex-Pr_2O_3 structure. While also the (111) surface of the cubic Pr_2O_3 lattice would exhibit hexagonal symmetry, the LEED pattern should reveal a 4×4 superstructure in this case,[28,38] in contrast to our experimental data.

When more than the initial layer is deposited, the (00) spot develops a six-fold symmetry instead of the threefold symmetry observed during the initial stage of the growth [see Fig. 2(b) for 95.5 eV electron energy]. The origin of this shape could be three-dimensional islands of hexagonal or triangular shape. The existence of such island structures is in agreement with the increasing roughness which was deduced from the continuous deposition experiment (Fig. 1).

The diffraction patterns for the sample prepared at 625 °C substrate temperature show a behavior which is very similar to the sample prepared at 550 °C (data not shown).

Quantitative information on the vertical and lateral roughness of the growing film can be extracted from analyzing (00) spot profiles measured at various electron energies. In the following, we restrict the analysis to coverages beyond the initial layer, when the growth starts to differ from a layer-by-layer growth mode. Figure 3(a) shows profile scans for two different electron energies that were recorded after depositing oxide at 550 °C with a nominal thickness of 0.9 and 1.2 nm (i.e., twice the coverage of the initial smooth layer), respectively. These profiles can be fitted as a superposition of three components: A sharp central peak, the width of which is limited by the instrumental resolution, and two shoulders (Henzler rings) around the central peak.

The shoulders represent ring-shaped distributions of scattering intensity around the (00) spot as illustrated in three-dimensional representations of the (00) spot in Fig. 3(b). The diameter $\Delta K_\parallel$ of the Henzler rings and their width do not depend on electron energy but on the amount of deposited oxide. The narrow shoulder almost merges with the central peak for the 0.9 nm thick oxide but is clearly visible when the oxide layer has a nominal thickness of 1.2 nm. Ring-shaped shoulders originate from characteristic lateral distances on a multilayer rough surface.[39] They may result, e.g., from a regular arrangement of islands leading to a narrow distribution of terrace widths. The diameter of the ring then correlates with the characteristic terrace widths $\langle\Gamma\rangle$ on the surface via[31,40]

$$\Delta K_\parallel = 2\pi/\langle\Gamma\rangle. \quad (1)$$

For the broad shoulder we determine values for $\langle\Gamma\rangle$ of ~8 nm for the 0.9 nm thick oxide and ~13 nm after depositing oxide with 1.2 nm nominal thickness, respectively. For the narrow shoulder we obtain $\langle\Gamma\rangle$ as ~33 nm for the 0.9 nm thick oxide and ~24 nm for the 1.2 nm thick film.

Information about the vertical roughness and characteristic step heights on the surface can be extracted from the central peak intensity normalized to the total (00) spot intensity (peak plus shoulders). This ratio is usually analyzed as a function of the vertical component of the electron scattering vector $K_\perp$. In the simple case of homoepitaxial layer-by-

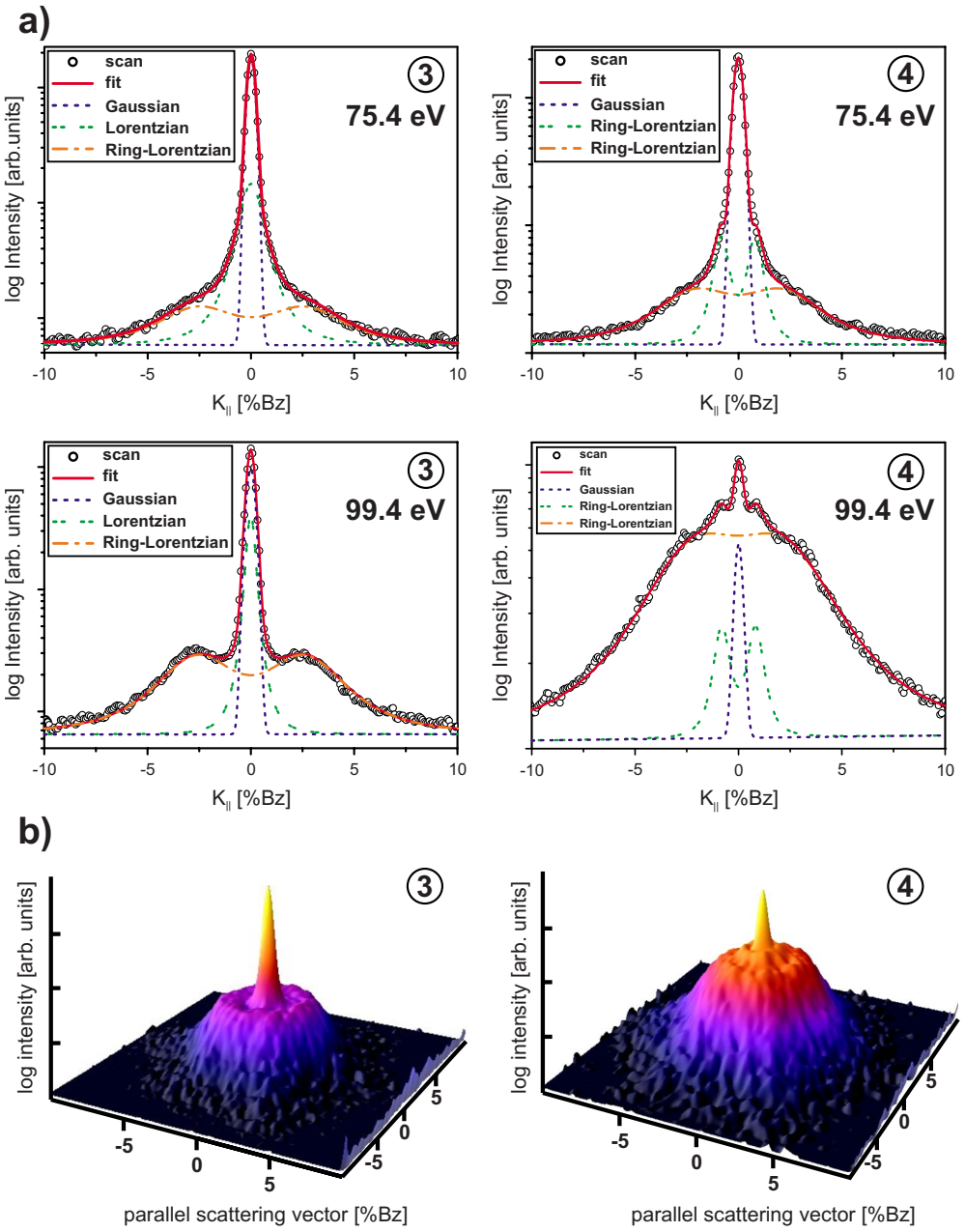

FIG. 3. (Color online) (a) Profiles of the specular diffraction spot at 0.9 nm (1.5 ML) and 1.2 nm (2 ML) film thickness for 75.4 and 99.4 eV, respectively. The profile is decomposed into three components (dashed lines). The solid line shows the resulting fit. (b) 3D illustration of the intensity of the specular beam. One and two Henzler rings, respectively, around the central peak are clearly visible.

layer growth with only one prevalent step height between adjacent terraces, the normalized intensity of the central peak depends on $K_\perp$ and on the coverage θ_1 of the growing layer as follows:[41]

$$G_{00}(K_\perp) = G_{\text{ideal}} \cdot [1 - 2\theta_1(1-\theta_1)(1-\cos K_\perp d)], \quad (2)$$

where G_{ideal} is the central peak intensity that would be measured for a perfectly flat surface and d denotes the prevalent step height. Based on the results of the (00) spot profile analysis for oxide deposition at 550 °C described above, the normalized peak intensity has been evaluated for several energies in the range 72–124 eV. The results are plotted in Fig. 4 versus the vertical scattering vector. While an oscillatory dependence is clearly visible, a fit to the data reveals significant deviations from a simple homoepitaxial model. First, in the investigated energy range the maxima do not reach a value close to 1 as would be expected for only one prevalent step height. Second, the succession of minima and maxima with increasing $K_\perp$ is not perfectly periodic. Both observations indicate that there are two or more different step heights prevalent on the surface. If many step heights were present, a value of 1 for $G(K_\perp)$ can be expected only for few definite values for $K_\perp$, i.e., for coincidence of constructive interference for all step heights. These electron energies, however, may be out of our experimental range.

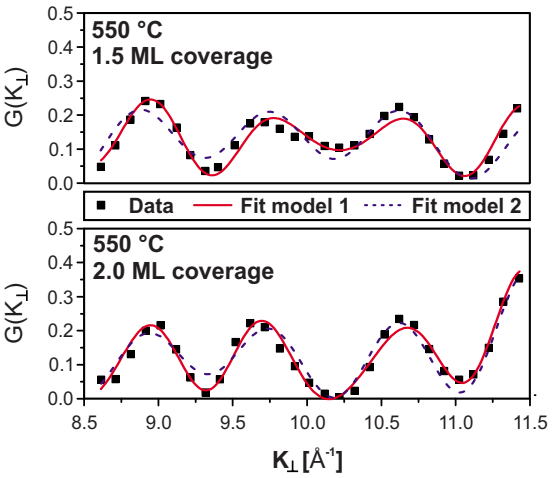

FIG. 4. (Color online) $G(K_\perp)$ curves for higher coverages [1.5 and 2.0 monolayers (ML)] of the sample prepared at 550 °C. The solid and dashed lines denote the results of a fitting procedure based on the models depicted in Fig. 5.

It is a reasonable assumption for the heteroepitaxial system under study that the different step heights of the silicon substrate and of the deposited oxide layer (cf. model 1 in Fig. 5) lead to the observed $G(K_\perp)$ curve. In fact, previous STM data (Ref. 19) indicate a roughening of the substrate during the formation of the initial layer during Pr-oxide deposition. Therefore, in addition to steps within the oxide layer (d), step heights of the initially flat substrate (s) may also be prevalent at the surface. As an alternative model for the origin of different step heights at the surface, we have also considered the formation of an inhomogeneous oxide layer composed of two separate domains or species with step heights d_1 and d_2, respectively. (cf. model 2 in Fig. 5). This model is motivated by evidence for chemical reactions at the interface which lead in some areas to significant material transport across the interface and silicide formation, as will be presented later.

Within the kinematic approximation of electron diffraction, both models provide a reasonable fit to the experimental data if electron scattering from six different surface atomic levels is considered and if both step heights (s and d or d_1 and d_2, respectively) and the surface fractions of the six different levels are used as fitting parameters. For simplicity, any influence of different scattering factors (form factor) for scattering from different levels, species, or at step edges is neglected

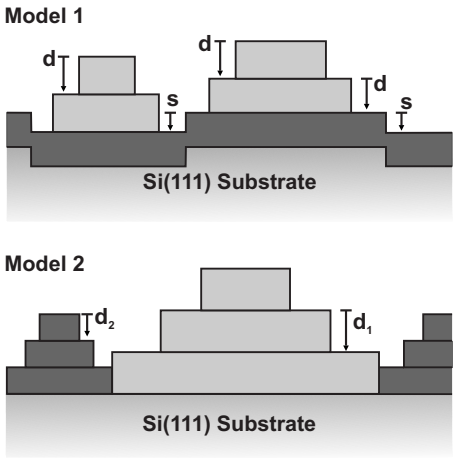

FIG. 5. Models used for fitting the experimental $G(K_\perp)$ curves. Two different step heights of the silicon substrate and of the deposited oxide layer (model 1) or an inhomogeneous oxide layer composed of two different domains (model 2) are assumed.

The resulting fits of both models are presented in Fig. 4 for two different oxide coverages. Model 1 (solid curve) provides the best fit with resulting step heights of $s=0.370$ nm [± 0.003] and $d=0.337$ nm [± 0.001]. Similar results are obtained by model 2 (dashed curve) with steps $d_1=0.352$ nm [± 0.03] and $d_2=0.327$ nm [± 0.07]. For both models the total coverage calculated from the surface fractions of the different atomic levels corresponds well to the actual coverage. The resulting root mean square (RMS) roughness of model 1 is in the range of 0.8 nm for both coverages (i.e., for coverages corresponding to 1.5 and 2.0 monolayers (ML). For model 2 the RMS is about 0.8 nm for the lower and about 1.3 nm for the higher coverage. An interpretation of the step heights resulting from the fitting procedure is difficult, probably because of the limitations of the model. They fit neither the Pr-Pr distance (~0.310 nm) nor one of the O-O distances (~0.395 nm, ~0.210 nm) reported for a hex-Pr_2O_3 layer in Si(111).[18] They somehow better fit the Pr-Pr distances of cub-Pr_2O_3 which lie in the range of 0.3–0.35 nm for the bulk crystal. Since silicate formation was observed in a previous study,[17] we also checked crystalline silicate structures (α-$Si_2Pr_2O_7$ and β-$Si_2Pr_2O_7$ reported by Felsche[42,43]) for layer distances comparable to the step heights of the SPA-LEED analysis, but no reasonable agreement was found. This may be taken as an indication of a more complicated (chemical) structure of the film obtained under the present conditions as compared to films prepared by MBE where an epitaxial layer-by-layer growth was observed previously. A more detailed model which could be expected to yield meaningful values for the step heights when fitted to the experimental data would have to take into account different scattering factors and phases for domains of different surface species. Such an elaborate analysis of the SPA-LEED data is beyond the scope and focus of the work presented here.

In summary, LEED reveals the formation of a closed and smooth initial layer at a nominal oxide thickness of 0.6 nm. In Ref. 19 an initial flat layer has been observed as well, grown from coalescing triangular islands with a preferred orientation. Those islands are also related to the triangularly shaped diffraction spots at oxide coverages below the completion of the initial layer. The data presented point to the initial growth of a hex-Pr_2O_3 layer as reported in other studies. The formation of cub-Pr_2O_3 domains at higher coverages cannot be excluded. SPA-LEED reveals that, above that initial layer, an ordered multilayer system starts to grow which exhibits two characteristic step heights. This might be due to a roughening of the film induced by chemical reactions in which also the silicon substrate is involved. To clarify such issues, the chemical composition of the growing film was investigated by XPS and XAS.

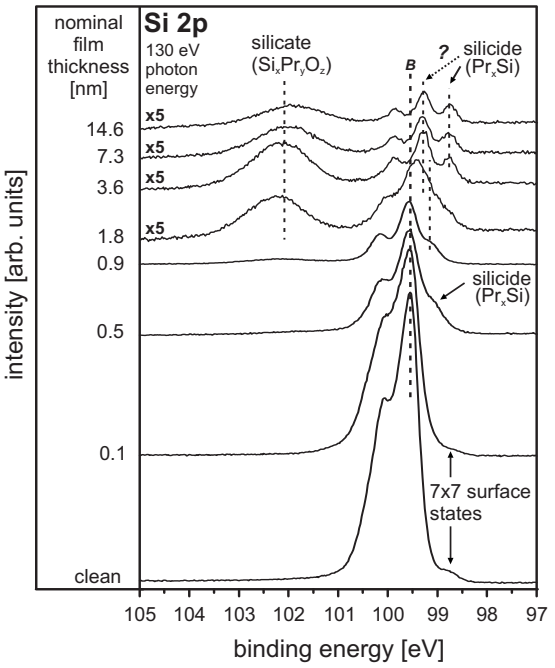

FIG. 6. Photoelectron spectra of the silicon 2p core level with different amounts of Pr_2O_3 deposited. Silicate and silicide related signals are clearly visible. ***B*** denotes the position of the bulk signal.

XPS

To monitor the changes in chemical composition of the surface during growth of the praseodymium oxide film, synchrotron radiation-based XPS and XAS experiments were performed. The spectra were recorded at room temperature after each preparation step in a stepwise deposition experiment at 600 °C substrate temperature. The amount of material deposited was increased stepwise to get an overview from small to large coverages.

The silicon 2p core level spectra are compiled in Fig. 6. The spectrum for the clean surface exhibits the spin orbit splitting of the 2p level and is broadened by the surface states of the (7×7) reconstruction. A further signal (~98.8 eV) also originating from adatoms of the surface reconstruction is visible at the low-binding energy side.[44]

After the first deposition step, the latter signal is still faintly visible and the Si 2p bulk signal has decreased in intensity due to covered parts of the substrate. The oxygen 1s spectrum after the first deposition, shown in Fig. 7(a), reveals a rather broad signal with a maximum at around 530.4 eV which is close to the binding energy of oxygen in the highly ionic environment of Pr-O-Pr bonds.[45,46] The observed value is about 0.7 eV higher, i.e., less oxidic than for bulk hex-Pr_2O_3.[17] The Pr $3d_{5/2}$ spectrum [Fig. 7(b)] has a main peak found at 933.8 eV which is 0.3 eV higher than for thicker Pr_2O_3 layers.[17,47] The signal exhibits a satellite structure which is due to final state hybridization effects of the O 2p and the Pr 4f level.[48] (The $3d_{3/2}$ signal shows qualitatively the same behavior and is not shown.) In conjunction with intra-atomic multiplet coupling effects, these effects also render the determination of the oxidation state of praseodymium complicated or even impossible. Theoretical models of those

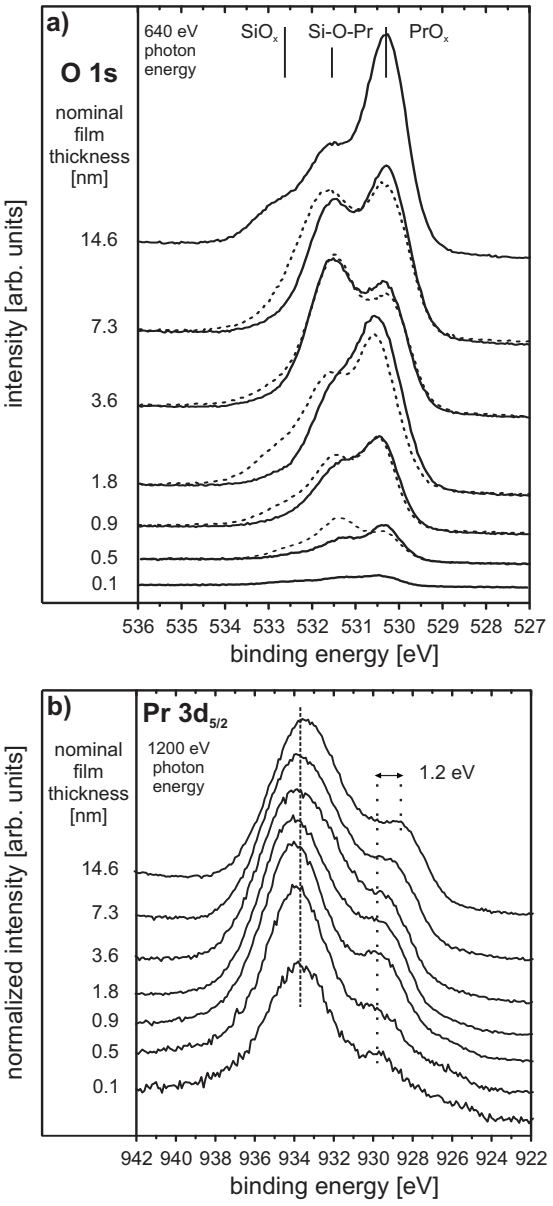

FIG. 7. Photoelectron spectra of a) oxygen 1s and b) praseodymium 3d core levels recorded at room temperature [directly after deposition (solid line) and after 2 h under UHV conditions (dashed line)]. The Pr 3d spectra are normalized to their intensity maximum.

effects have been discussed in the literature but are still under debate (for detailed information see Refs. 22, 45, and 48–52).

So, while the spectra after the first deposition step are consistent with the growth of a praseodymium oxide-like structure in the early stages of growth, the formation of silicides is observed after the next step (0.5 nm), which is close to the formation of the monolayer. Silicide formation is apparent in the Si 2p spectrum exhibiting a shoulder around 99.2 eV. (Silicides form large inclusions in the silicon substrate as will be shown later in the TEM section). According to Schmeißer *et al.*[29] silicides are expected only to form during praseodymium oxide growth under very oxygen deficient conditions on Si(001) surfaces. Watahiki *et al.* very recently reported silicide formation on Si(001) under very similar

growth conditions compared to ours.[53] Up to now, the formation of silicide structures on Si(111), during praseodymium oxide deposition has been reported only upon heating to temperatures higher than 700 °C.[54]

In the oxygen spectrum at 0.5 nm film thickness, the signal due to Pr-O-Pr configurations dominates (530.4 eV), similar to the data for the 0.1 nm thick film. Nevertheless, other contributions are clearly discernible, now: On the high-binding energy side around 532.5 eV, a small signal is detectable which is typical for the more covalently bound oxygen in SiO_x compounds. Between this and the dominant Pr-O-Pr signal, a further contribution appears which, according to the literature, arises from Si-O-Pr bonding configurations,[17,46,55] as expected at the substrate-oxide interface. Concomitantly, in the Pr 3d spectrum, a small shift of the main peak to higher-binding energies about 0.1 eV is visible for a film thickness of 0.5 nm.

Interestingly, the film is chemically not stable even after cooling to room temperature. O 1s spectra recorded 2 h *after* the initial one [dashed lines in Fig. 7(a)] reveal an increase in oxygen in Si-O-Pr bonds at expense of oxygen in Pr-O-Pr bonds, indicating that a reaction at the interface has occurred.

At coverages beyond one monolayer (0.9 and 1.8 nm film thickness), the Pr-oxide signal (530.5 eV) remains dominant not only immediately after the deposition but also after 2 h (dashed lines). Note, however, that the silicate and SiO_x content increases over time here as well. The Si 2p spectrum (Fig. 6) at 0.9 nm reveals that the silicide (Pr_xSi) signal increases *together* with a broad signal slightly above 102 eV binding energy arising from silicate (Si-O-Pr) bonds.

After deposition of oxide of 1.8 nm nominal thickness, a shift of the main peak in the Si 2p spectrum is observed and the signal becomes broader. There are two possible explanations for this observation: First, the main peak could still result from elemental Si and is shifted toward lower-binding energy due to silicate formation and resulting band bending as reported for other systems.[56,57] Second, the structure of the signal could be explained by a further contribution of silicide species of different stoichiometry, the formation of which is discussed by Netzer.[58] Together with remaining intensity from elemental Si this possibly explains the broadening of the signal. Almost no changes occur in the Pr 3d spectra after depositing 0.9 and 1.8 nm except for a better resolution of the satellite structure.

The next deposition step results in a nominal film thickness of 3.6 nm. It is important to note that now the deposition time is already about 30 min, during which the sample is kept at elevated temperatures (600 °C). Hence, silicon diffusion is promoted which leads to a dominating silicate (Si-O-Pr) contribution in the O 1s spectrum even directly after the deposition is finished (solid line). The Pr 3d spectrum is broadened by the silicate formation, but no pronounced shift towards the previously reported binding energy for Pr silicate at 934.8 eV[17,22,23] is observed. This observation points to a nonstoichiometric silicate phase due to the deficit of oxygen during deposition. In the Si 2p spectrum, the silicate signal around 102 eV binding energy is also increased in intensity. The main peak of the Si 2p signal group shifts further about 1.4 eV to lower-binding energy and becomes narrower again. This observation may be again

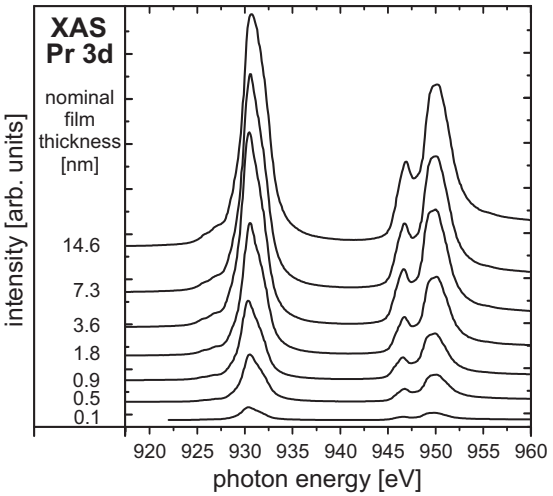

FIG. 8. X-ray absorption spectra of the Pr 3d edge. The spectra give evidence that Pr^{3+} is prevalent throughout the whole film.

explained in two ways. On the one hand the shift can be due to ongoing band bending resulting from a thicker silicate layer. On the other hand the signal can be decomposed in at least three spin orbit pairs due to different silicide phases, namely, Pr_5Si_3, PrSi, and Pr_3Si_5.[58] The origin of the observed shifts in the Si 2p spectra is an open question at this point and will be the subject of further investigations.

Although the deposition time for the last two steps is about one and two hours, respectively, the Pr oxide signal still dominates the O 1s spectra. The suppression of silicate formation can be explained by the large film thickness restraining diffusion of Si. In the Pr 3d spectra, a small shift toward lower-binding energy values (about 0.44 to 933.6 eV) is detectable and results in a binding energy which is close to the value observed for bulk Pr_2O_3 on Si(111) (933.5 eV).[17] A stronger separation of the satellite with respect to the main signal is visible as well, pointing to a higher amount of stoichiometric Pr oxide on the surface.[48]

In summary, the XPS study reveals the formation of a praseodymium-oxide-like initial layer. In the following, an interface reaction occurs due to silicon diffusion which even proceeds at room temperature. Although the Pr 3d signal is at a Pr_2O_3 position for the 14 nm film, the oxygen 1s spectrum reveals the presence of silicate and SiO_x species but a stoichiometric silicate ($Si_2Pr_2O_7$) is probably *not* formed. Even silicide entities are present up to high coverages, as evidenced by the silicon 2p spectra.

XAS

X-ray absorption spectroscopy is a useful tool to obtain information on the unoccupied electronic states of a system. By analyzing the extended fine structure of such absorption spectra, even the local geometry of a certain element can be determined. In the following, absorption spectra from the praseodymium 3d and oxygen 1s edge are presented and discussed.

In Fig. 8 the absorption spectra from the Pr-3d edge are compiled. Two signal groups due to 3d-4f transitions cen-

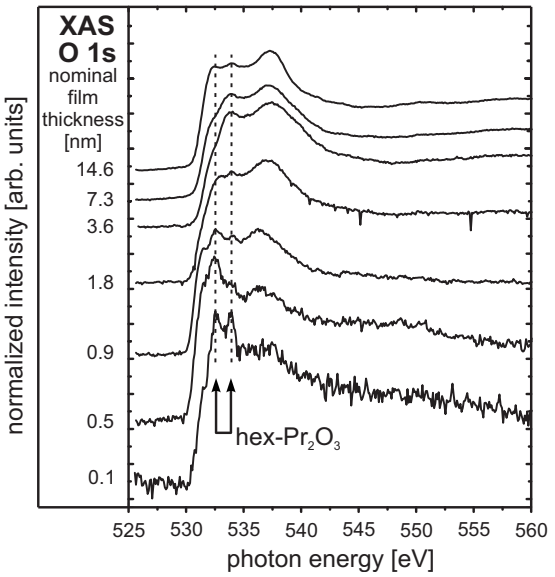

FIG. 9. X-ray absorption spectra of the oxygen 1s edge (normalized to the intensity maximum). A characteristic double-peak structure (most pronounced for the submonolayer coverage) is visible indicating the presence of the hex-Pr_2O_3 structure.

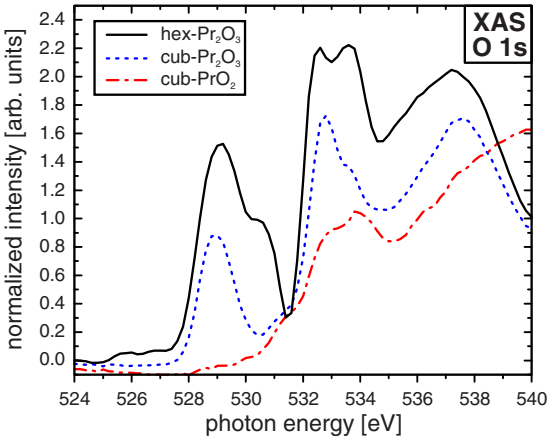

FIG. 10. (Color online) X-ray absorption spectra of the O 1s edge for a 7 nm film of hex-Pr_2O_3 (Solid line), cub-Pr_2O_3 (dotted line) and cub-PrO_2 (dash-dotted line). The spectra have been measured by O. Seifarth at the ASAM end station at BESSY II (Berlin/Germany). For details of the measurement see ref. 65.

tered around 930.4 and 950 eV are observed, respectively. The difference in energy approximately corresponds to the $3d_{3/2}$-$3d_{5/2}$ spin-orbit splitting. A more detailed interpretation of the Pr 3d spectra is complicated due to the covalent hybridization effects of the final state and intra-atomic multiplet interactions which have to be taken into account and give rise to a special fine structure.[48,49,51,59,60] For the purpose of this study, we use the Pr 3d XAS data just as a characteristic fingerprint to determine the dominating valence state in the growing film. If compared to other data of materials containing trivalent Pr ions,[51,59,61,62] it can be clearly concluded that the presented spectra result from a Pr^{3+} species prevailing throughout the whole film. Characteristic fine structure features are missing which would originate from an additional d-electron transition of tetravalent Pr species to the empty 4f level.

The spectra from the oxygen 1s edge are displayed in Fig. 9. In the first spectrum the absorption starts at 530 eV photon energy. A characteristic double-peak structure occurs with peaks at 532.8 and 533.9 eV, respectively. As pointed out by Schmeißer *et al.*,[63,64] absorptions in this range are due to oxygen 2p to Pr 4f charge transfer transitions and thus sensitive to the specific ligand configurations. Figure 10 displays results for O1s XAS obtained by O. Seifarth *et al.* for single crystalline cub-Pr_2O_3(111), hex-Pr_2O_3(0001), and cub-PrO_2(111) films of ~7 nm thickness on Si(111), respectively. Details of this study are reported in Ref. 65. Whereas for cub-Pr_2O_3 no double-peak structure is observed in Fig. 10, such a structure is observed for the hex-Pr_2O_3 film with peaks at 532.6 and 533.6 eV, respectively. Taking the spectra of Fig. 10 as a reference it can be concluded that a structure similar to hex-Pr_2O_3 forms in the initial stages of the film growth in agreement with the data discussed in the previous sections.

When the coverage is increased to and beyond one monolayer, the double-peak structure becomes less pronounced but never vanishes completely. It is visible in particular at the highest-oxide coverage, pointing to the existence of hex-Pr_2O_3 domains throughout the whole film. However, a comparison of the x-ray absorption (XA) spectra for 0.5 and 0.9 nm oxide thickness with the data presented in Fig. 10 indicates that at these coverages also domains of cubic Pr_2O_3 structure are present on the surface. The identification of clear fingerprints in the XAS data becomes more tedious at higher-oxide coverages. For instance, the shoulder at around 537.5 eV photon energy increases in intensity. Since such a signal was reported for both, Pr_2O_3 structures as well as for Pr silicate layers,[63–65] however, a clear assignment is not possible.

Finally, it should be mentioned that an absorption signal observed for the bulk Pr_2O_3 phases at 529.5 eV is missing in our spectra. An absorption signal at this position has also been reported for Ceria samples.[66] In a localized-electron picture this signal results from an $O1s^2 -> Ce4f^0$ transition, allowed by the O2pCe4f hybridization. For a $4f^1$ final state [$Ce(IV)O_2$] such a signal is observed, while the signal is absent for a $4f^2$ [$Ce(III)_2O_3$] final state. In case of praseodymium there is one more electron present, leading to an inverse behavior regarding the oxidation state (Fig. 10). The signal is again absent for the $4f^2$ final state, which now corresponds to the Pr(IV) valency in PrO_2, but is observed for the $4f^3$ final state in case of the Pr(III) valency in Pr_2O_3. However, although the Pr3d XAS measurements revealed Pr^{3+} as the prevalent species in the film the signal at 529.5 eV is absent in the O1s spectra. This could probably be due to the large amount of silicon present in the film leading both to silicate and silicide formation. For the case of silicate, Schmeißer *et al.* proposed that the absence of the signal is due to covalent contributions and charge transfer complexes from the Si 3p states.[63,64] In our case, however, the signal is completely missing although Pr_2O_3 domains exist in addition to Si-O-Pr bonds. This could be due to the fact that oxide and silicate areas grow in close proximity.

In summary, the XAS data support the assumption of an initial growth of hex-Pr_2O_3 in the submonolayer range. Also

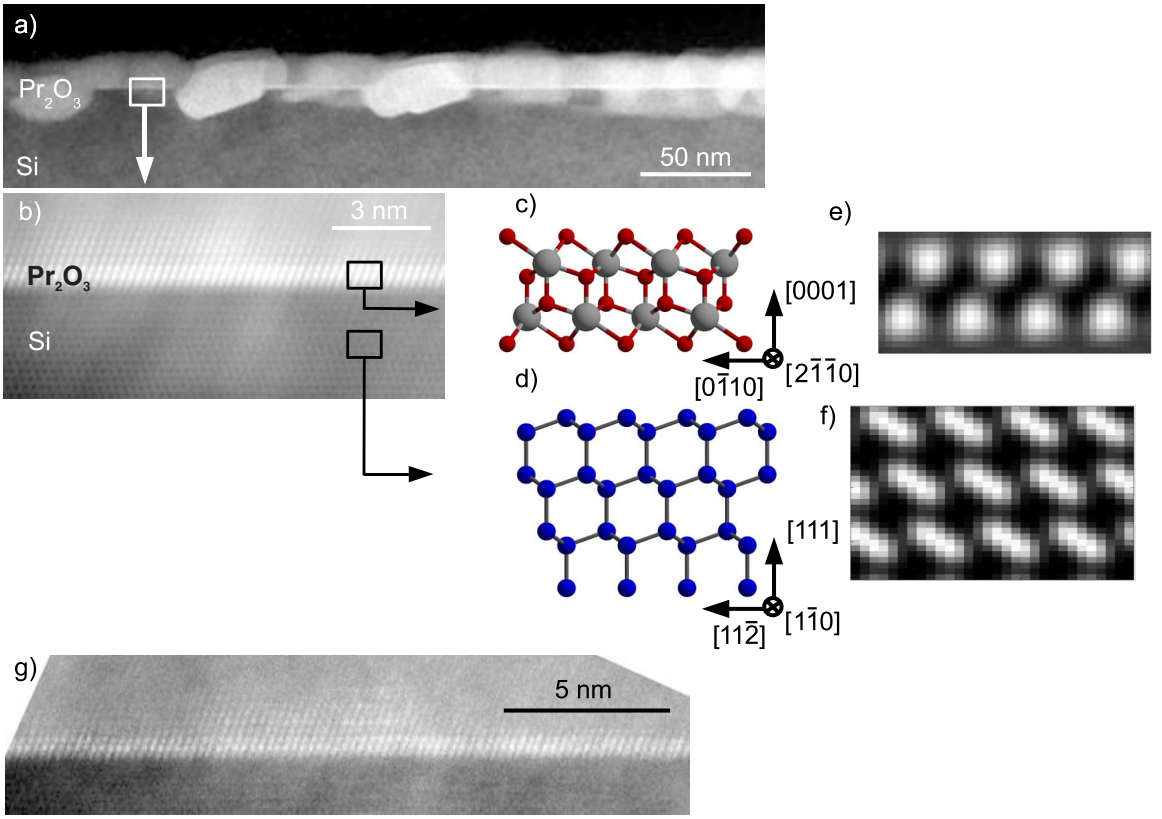

FIG. 11. (Color online) (a) STEM image of a continuously deposited film of 14 nm thickness. Inclusions, most likely consisting out of silicide, and a thin bright line at the interface are visible; (b) HRSTEM image of the interface region; (c) and (d) structure model for hex-Pr_2O_3 on Si(111) according to ref. 18 used for the simulation in (e) and (f); g) unfiltered HRSTEM image.

domains of the cubic Pr_2O_3 structure seem to coexist when the first layer is completed which is later overgrown by a mixture of silicate and oxide domains.

TEM

To complement the study by microscopic data, cross sectional STEM of a film of 14 nm thickness, continuously deposited at 600 °C substrate temperature, was conducted. The overview in Fig. 11(a) reveals that a continuous layer has formed on top of the Si substrate. However, the deposited layer is not homogeneous on the lateral scale of several 100 nm. Two distinct features are clearly visible: a continuous thin bright line at the interface between the substrate (bottom) and the deposited film (top) and inclusions with lateral dimensions in the range of some 10 nm which extend from the top of the oxide layer to ~10 nm into the silicon substrate below the bright line. These inclusions are crystalline and consist most likely of silicide entities as indicated by XPS. Similar inclusions extending deep into the substrate have also been observed for the Nd_2O_3/Si(001) system under similar growth conditions.[67]

The brightness of the line above the Si surface indicates the presence of heavy Pr atoms in that layer, leading to the assumption based on the LEED that the bright features correspond to the Pr positions in the initial Pr_2O_3 monolayer. The assumption is confirmed by means of a noise-filtered high-resolution STEM (HRSTEM) image [Fig. 11(b)] of the region indicated in Fig. 11(a). The width of the bright line corresponds well to the nominal thickness of 0.6 nm of the smooth initial layer. In order to relate the experimental TEM image to a crystal structure, simulations have been carried out employing the StemSim program[68] using the structures depicted in Figs. 11(c) and 11(d) for hex-Pr_2O_3 and Si, respectively. The resulting *Z*-contrast images of both structures are shown in Figs. 11(e) and 11(f). The results demonstrate that the initial bright layer comprises two layers of Pr atoms which show reasonable agreement with the hex-Pr_2O_3 structure.

There are some regions with more than two Pr layers faintly visible [cf. Fig. 12(a)]. Close inspection reveals that the stacking of layers in these areas with local coverages beyond the initial monolayer is not hexagonal but cubic. Comparison of the TEM image to the hexagonal and cubic structures of the sesquioxide is again made by simulation on the basis of the crystal structures shown in Figs. 12(b) and 12(c). For Pr_2O_3/Si(111) the [1–10] direction in Si is parallel to the [2–1-1 0] direction in hex-Pr_2O_3 and [1–10] direction in cub-Pr_2O_3, respectively.[18,28] The growth directions are [0001] and [111], respectively, so that in both phases the configuration of the first two atomic layers is very similar with respect to the Pr positions. The Pr positions clearly differ in the third layer, since the hex-Pr_2O_3 phase exhibits an ABA stacking sequence, while the cub-Phase on Si(111) is characterized by an ABC sequence (Type-B stacking).[24] On basis of our TEM data, we exclusively find multilayer re-

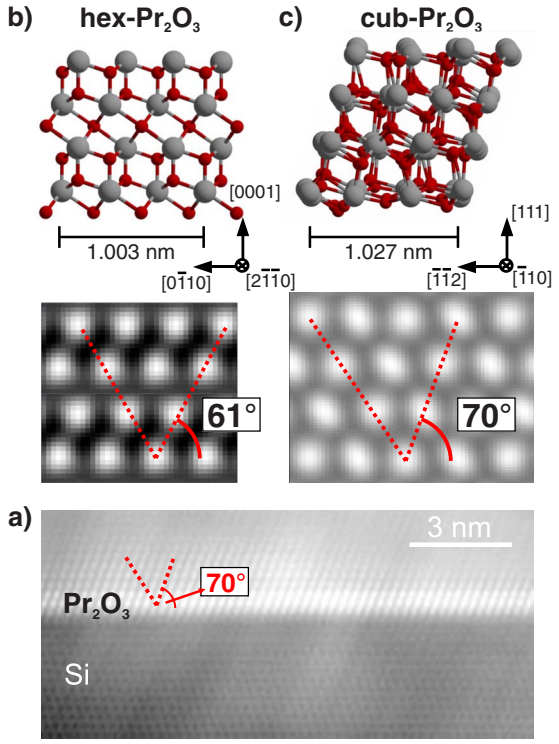

FIG. 12. (Color online) (a) HRSTEM image of the interface region as in Fig. 11; (b) and (c) ball and stick models of the cubic and hexagonal crystal structure of Pr_2O_3, respectively, along with the results of the simulation of the corresponding TEM image.

gions with type-B stacking, confirming the presence of cub-Pr_2O_3 domains inferred from the XA spectra. These multilayer structures may be related to the three-dimensional ordered islands indicated by SPA-LEED.

IV. SUMMARY AND CONCLUSIONS

The growth of praseodymium oxide on a (7×7)-Si(111) substrate has been investigated using small deposition rates and low-oxygen partial pressures. Structural information has been obtained by SPA-LEED and TEM, whereas XPS and XAS were employed to clarify the chemical composition of the film.

The results clearly show differences to samples prepared under higher-oxygen partial pressures and with higher-deposition rates. Instead of layer-by-layer growth, only the formation of an initial flat monolayer comprising two atomic layers of Pr is observed before continuous roughening occurs. Our XPS results confirm that the initial flat layer is composed of Pr_2O_3. From the submonolayer coverage regime up to completion of the initial monolayer the LEED pattern and XAS spectra both show properties expected for the hex-Pr_2O_3 phase, in accordance with previous studies.[18,19] An arrangement of the praseodymium and oxygen atoms within the initial layer according to the hex-Pr_2O_3 phase is probably favored due to a small lattice mismatch with respect to the substrate. Libralesso *et al.*[19] reported the formation of triangular islands with a preferred orientation in the submonolayer regime. The formation of triangular islands in the first stages of the growth is consistent with our electron diffraction experiments which revealed diffraction spots of triangular shape below 1 ML.

At coverages around 1 ML and beyond, the XAS spectrum shows contributions from the cubic phase of the sesquioxide. At monolayer coverage, however, no (4×4) superstructure spots are observed in LEED which would be expected if the entire initial flat layer exhibited the cub-Pr_2O_3 structure. Given the STEM data which reveal domains of ABC stacking sequence (rotated 180° with respect to the silicon substrate) of the Pr-atoms typical for cub-Pr_2O_3 in those areas where apparently multilayer islands have formed, we assume that domains of the cubic phase build up in areas with local coverages beyond one monolayer, i.e., where three-dimensional oxide islands form on top. While TEM as a local probe did not reveal islands with ABA stacking of Pr layers within the available data, both cubic and hexagonal domains seem to *coexist* throughout the film also at higher coverages, as the XAS data indicate.

Chemical reactions at the interface between oxide layer and silicon substrate even add more complexity to the structural details of the Pr_2O_3 layer grown at low-deposition rate and low-oxygen partial pressure. The initial layer is overgrown by a mixture of the oxide and a silicate due to silicon diffusion into the film. At the same time, a silicide phase forms resulting in large silicide inclusions in the film. Whereas the silicide grows in the form of large crystalline inclusions, the Pr_2O_3 and silicate areas are possibly formed in close proximity and cannot be resolved in TEM.

A similar behavior was recently reported by Libralesso *et al.*[69] for the growth of Pr_2O_3 on Si(001) (with a total film thickness of 2.5 nm) when applying low-deposition rates. Here, a cub-Pr_2O_3 monolayer was first formed and then overgrown by silicate. Yet, no silicide formation has been observed by these authors due to higher-oxygen partial pressures (5×10^{-8} mbar) applied in their preparations. A possible explanation for the initial formation of a Pr_2O_3 layer on top of the silicon substrates could be that such layers are thermodynamically more favorable than the direct formation of a silicate, a conclusion which is in agreement with theoretical calculations for growth on Si(001)[70,71]

In conclusion, our study shows that the growth of reactive oxides, such as praseodymia, on supports which can be easily oxidized, such as Si, may be strongly influenced by the oxygen partial pressure during deposition and the deposition rates. Whereas for Pr_2O_3 growth on Si(111), smooth films and a layer-by-layer growth is observed under conditions typical for MBE, chemical reactions with the Si support lead to silicate and silicide formation in the growing film in case of low-deposition rates and low-oxygen partial pressures typical of UHV model studies. So care has to be taken to avoid structural and chemical heterogeneity under such conditions which would hamper the investigation of fundamental properties relevant for technical applications, such as catalysis or microelectronics. One possibility (besides careful control of the oxygen partial pressure during epitaxial growth) reported for Si(001) is silicon co-evaporation to enforce the formation of a crystalline silicate interface blocking the further diffusion of Si into the growing film.[72]

ACKNOWLEDGMENTS

We thank the staff at MAX-lab for their assistance. Financial support from the Fonds der Chemischen Industrie and the University Bremen (Zentrale Forschungsförderung) is gratefully acknowledged. A.S. thanks the Swedish Science Council (VR) for financial support. A.S. is grateful for financial support from the postgraduate international program (PIP, University of Bremen).

*Corresponding author. mbaeumer@uni-bremen.de

[1] H. Borchert, Y. V. Frolova, V. V. Kaichev, I. P. Prosvirin, G. M. Alikina, A. I. Lukashevich, V. I. Zaikovskii, E. M. Moroz, S. N. Trukhan, V. P. Ivanov, E. A. Paukshtis, V. I. Bukhtiyarov, and V. A. Sadykov, J. Phys. Chem. B **109**, 5728 (2005).

[2] G. Adachi and N. Imanaka, Chem. Rev. (Washington D. C.) **98**, 1479 (1998).

[3] S. J. Huang, A. B. Walters, and M. A. Vannice, Appl. Catal., B **17**, 183 (1998).

[4] G. V. Antoshin, Kh. M. Minachev, and R. V. Dmitriev, Russ. Chem. Bull. **16**, 1793 (1967).

[5] T. Schroeder, A. Giussani, J. Dabrowski, P. Zaumseil, H.-J. Müssig, O. Seifarth, and P. Storck, Phys. Status Solidi C **6**, No. 3, 653 (2009).

[6] Y. Zhao, M. Toyama, K. Kita, K. Kyuno, and A. Toriumi, Appl. Phys. Lett. **88**, 072904 (2006).

[7] K. Otsuka and M. Kunitomi, J. Catal. **105**, 525 (1987).

[8] Y. Takasu, M. Matsui, H. Tamura, S. Kawamura, Y. Matsuda, and I. Toyoshima, J. Catal. **69**, 51 (1981).

[9] Y. Takasu, M. Matsui, and Y. Matsuda, J. Catal. **76**, 61 (1982).

[10] E. M. Kennedy and N. W. Cant, Appl. Catal. **75**, 321 (1991).

[11] S. K. Bhaskaran and V. T. Bhat, React. Kinet. Catal. Lett. **75**, 239 (2002).

[12] Y. Borchert, P. Sonström, M. Wilhelm, H. Borchert, and M. Bäumer, J. Phys. Chem. C **112**, 3054 (2008).

[13] C. T. Campbell, Surf. Sci. Rep. **27**, 1 (1997).

[14] C. R. Henry, Surf. Sci. Rep. **31**, 231 (1998).

[15] M. Bäumer and H. J. Freund, Prog. Surf. Sci. **61**, 127 (1999).

[16] T. Weisemoeller, C. Deiter, F. Bertram, S. Gevers, A. Giussani, P. Zaumseil, T. Schroeder, and J. Wollschlager, Appl. Phys. Lett. **93**, 032905 (2008).

[17] A. Schaefer, T. Schroeder, G. Lupina, Y. Borchert, J. Dabrowski, C. Wenger, and M. Bäumer, Surf. Sci. **601**, 1473 (2007).

[18] N. Jeutter, A. Sidorenko, A. Stierle, and W. Moritz, Appl. Phys. Lett. **90**, 062906 (2007).

[19] L. Libralesso, T. Schroeder, T. L. Lee, and J. Zegenhagen, Surf. Sci. **598**, L347 (2005).

[20] T. Schroeder, T.-J. Lee, L. Libralesso, I. Jounard, J. Zegenhagen, P. Zaumseil, C. Wenger, G. Lupina, G. Lippert, J. Dabrowski, and H.-J. Müssig, J. Appl. Phys. **97**, 074906 (2005).

[21] B. P. Tinkham, M. Takahashi, B. Jenichen, T. Watahiki, W. Braun, and K. H. Ploog, Semicond. Sci. Technol. **21**, 1552 (2006).

[22] A. Fissel, J. Dabrowski, and H. J. Osten, J. Appl. Phys. **91**, 8986 (2002).

[23] H. J. Müssig, J. Dabrowski, K. Ignatovich, J. P. Liu, V. Zavodinsky, and H. J. Osten, Surf. Sci. **504**, 159 (2002).

[24] J. P. Liu, P. Zaumseil, E. Bugiel, and H. J. Osten, Appl. Phys. Lett. **79**, 671 (2001).

[25] E. J. Tarsa, J. S. Speck, and D. R. Mc, Appl. Phys. Lett. **63**, 539 (1993).

[26] H. J. Osten, E. Bugiel, and A. Fissel, Solid-State Electron. **47**, 2161 (2003).

[27] H. J. Osten, J. P. Liu, E. Bugiel, H. J. Müssig, and P. Zaumseil, Mater. Sci. Eng., B **87**, 297 (2001).

[28] T. Schroeder, P. Zaumseil, G. Weidner, C. Wenger, J. Dabrowski, H. J. Müssig, and P. Storck, J. Appl. Phys. **99**, 014101 (2006).

[29] D. Schmeißer, J. Dabrowski, and H. J. Müssig, Mater. Sci. Eng., B **109**, 30 (2004).

[30] U. Scheithauer, G. Meyer, and M. Henzler, Surf. Sci. **178**, 441 (1986).

[31] M. Horn von Hoegen, Z. Kristallogr. **214**, 591 (1999).

[32] J. Wollschläger, J. Falta, and M. Henzler, Appl. Phys. A **50**, 57 (1990).

[33] I. V. Markov, *Crystal Growth for Beginners* (World Scientific, Singapore, 1995).

[34] M. Henzler, H. Busch, and G. Friese, in *Kinetics of Ordering and Growth at Surfaces*, edited by M. G. Lagally (Plenum, New York, 1990), p. 101.

[35] J. Wollschläger and A. Meier, Appl. Surf. Sci. **104-105**, 392 (1996).

[36] V. Zielasek, A. Büssenschütt, and M. Henzler, Phys. Rev. B **55**, 5398 (1997).

[37] Low-energy electrons are sensitive to the threefold (bulk) diamond structure of Si(111) although the penetration depth is very small. Thus, one often observes the threefold symmetry of higher-order diffraction peaks. The diffraction from hex-Pr_2O_3(0001) or cub-Pr_2O_3(111), however, exhibits six-fold symmetry. Therefore, Pr_2O_3 islands which prevent the penetration of the electrons in the Si substrate underneath the oxide islands act like "holes" which cause the diffuse threefold shape of the diffuse diffraction.

[38] S. Gevers, T. Weisemoeller, B. Zimmermann, F. Bertram, C. Deiter, and J. Wollschläger, J. Phys. Condens. Matter **21**, 175408 (2009).

[39] P. R. Pukite, C. S. Lent, and P. I. Cohen, Surf. Sci. **161**, 39 (1985).

[40] J. Wollschläger, Surf. Sci. **383**, 103 (1997).

[41] C. S. Lent and P. I. Cohen, Surf. Sci. **139**, 121 (1984).

[42] J. Felsche, Naturwiss. **57**, 452 (1970).

[43] J. Felsche, Naturwiss. **57**, 669 (1970).

[44] C. J. Karlsson, E. Landemark, Y.-C. Chao, and R. I. G. Uhrberg, Phys. Rev. B **50**, 5767 (1994).

[45] S. Lütkehoff, M. Neumann, and A. Slebarski, Phys. Rev. B **52**, 13808 (1995).

[46] G. Lupina, T. Schroeder, J. Dabrowski, C. Wenger, A. Mane, G. Lippert, and H. J. Müssig, Appl. Phys. Lett. **87**, 092901 (2005).

[47] A. Fissel, H. J. Osten, and E. Bugiel, J. Vac. Sci. Technol. B **21**, 1765 (2003).

[48] A. Kotani and H. Ogasawara, J. Electron Spectrosc. Relat.

Phenom. **60**, 257 (1992).
[49] L. Petit, A. Svane, Z. Szotek, and W. M. Temmerman, Phys. Rev. B **72**, 205118 (2005).
[50] H. Ogasawara, A. Kotani, R. Potze, G. A. Sawatzky, and B. T. Thole, Phys. Rev. B **44**, 5465 (1991).
[51] B. T. Thole, G. van der Laan, J. C. Fuggle, G. A. Sawatzky, R. C. Karnatak, and J. M. Esteva, Phys. Rev. B **32**, 5107 (1985).
[52] A. Bianconi, A. Kotani, K. Okada, R. Giorgi, A. Gargano, A. Marcelli, and T. Miyahara, Phys. Rev. B **38**, 3433 (1988).
[53] T. Watahiki, B. P. Trinkham, B. Jenichen, R. Shayduk, W. Braun, and H. Ploog, Appl. Surf. Sci. **255**, 758 (2008).
[54] N. M. Jeutter, M. Hennemeyer, R. Stark, A. Stierle, and W. Moritz, Mater. Sci. Semicond. Process. **9**, 1079 (2006).
[55] G. Lupina, T. Schroeder, J. Dabrowski, C. Wenger, A. U. Mane, H. J. Müssig, P. Hofmann, and D. Schmeißer, J. Appl. Phys. **99**, 114109 (2006).
[56] A. Sandell, P. G. Karlsson, J. H. Richter, J. Blomquist, P. Uvdal, and T. M. Grehk, Appl. Phys. Lett. **88**, 132905 (2006).
[57] J. H. Richter, P. G. Karlsson, B. Sanyal, J. Blomquist, P. Uvdal, and A. Sandell, J. Appl. Phys. **101**, 104120 (2007).
[58] F. P. Netzer, J. Phys.: Condens. Matter **7**, 991 (1995).
[59] K. Binder and D. P. Landau, Phys. Rev. B **37**, 1745 (1988).
[60] H. Ogasawara, A. Kotani, K. Okada, and B. T. Thole, Phys. Rev. B **43**, 854 (1991).
[61] G. Kaindl, G. Kalkowski, W. D. Brewer, B. Perscheid, and F. Holtzberg, J. Appl. Phys. **55**, 1910 (1984).
[62] Z. Hu, G. Kaindl, H. Ogasawara, A. Kotani, and I. Felner, Chem. Phys. Lett. **325**, 241 (2000).
[63] D. Schmeißer, F. Zheng, V. Perez-Dieste, F. J. Himpsel, R. LoNigro, R. G. Toro, G. Malandrino, and I. L. Fragalà, Mater. Sci. Eng., C **26**, 1122 (2006).
[64] D. Schmeißer and H. J. Müssig, Mater. Sci. Semicond. Process. **7**, 221 (2004).
[65] O. Seifarth, J. Dabrowski, P. Zaumseil, S. Müller, D. Schmeißer, H. J. Müssig, and T. Schroeder, J. Vac. Sci. Technol. B **27**, 271 (2009).
[66] D. R. Mullins, S. H. Overbury, and D. R. Huntley, Surf. Sci. **409**, 307 (1998).
[67] A. Fissel, Z. Elassar, O. Kirfel, E. Bugiel, M. Czernohorsky, and H. J. Osten, J. Appl. Phys. **99**, 074105 (2006).
[68] A. Rosenauer and M. Schowalter, in *Springer Proceedings in Physics*, edited by A. G. Cullis (Springer, New York, 2008), Vol. 120.
[69] L. Libralesso, T. L. Lee, and J. Zegenhagen, Appl. Phys. Lett. **90**, 222905 (2007).
[70] H. J. Osten, J. Dabrowski, H. J. Müssig, A. Fissel, and V. Zavodinski, in *Predictive Simulation of Semiconductor Processing*, edited by J. Dabrowski and E. Weber (Springer, New York, 2004), Vol. 72, p. 259.
[71] J. Dabrowski and V. Zavodinsky, in *Proceedings of the NIC Symposium 2004*, edited by D. Wolf, G. Münster, and M. Kremer (John von Neumann Institut für Computing, Jülich, Germany, 2003), Vol. 20, p. 171.
[72] T. Watahiki, B. P. Tinkham, B. Jenichen, W. Braun, and K. H. Ploog, J. Cryst. Growth **301-302**, 381 (2007).